HEFAT2010
7th International Conference on Heat Transfer, Fluid Mechanics and Thermodynamics
19-21 July 2010
Antalya, Turkey

EXPERIMENTAL INVESTIGATION OF THE INTERACTION BETWEEN SLOPE FLOWS AND URBAN HEAT ISLANDS VIA IMAGE ANALYSIS TECHNIQUES

Cenedese A., Giorgilli M. and Moroni M.*
*Author for correspondence
Department of Hydraulics, Transportations and Roads,
Sapienza University of Rome,
Italy,
E-mail: monica.moroni@uniroma1.it

ABSTRACT

This paper is focused on the interaction of slope flows with urban heat islands, which are studied here by means of laboratory simulations. During the day, sunlight heats slope surfaces more than the adjacent air, resulting in a wind flow in the upslope direction: 'anabatic wind'. When the slope cools down rapidly during the night, the direction of the wind flow is reversed: 'katabatic wind'. These winds influence the strength and form of the UHIs, and its mutual interaction is studied in this paper. The combined use of thermocouples and image analysis techniques provides the simultaneous measurement of temperature and velocity components. In particular the velocity field for different time instants from the beginning of the experiments, the thickness of fluid layers interested by slope flows, the height of the plume caused by the urban heat island and its position in the anabatic and case have been determined.

INTRODUCTION

The local atmospheric circulation influences dispersion phenomena on urban scale. Due to the high concentration of human activities and buildings, temperatures in urban regions tend to be higher compared to the surrounding rural areas. Such a warm area is called an 'Urban Heat Island' (UHI). In this study, the interaction of these UHIs with an adjacent mountainous region is studied, since many (large- scale) cities are located in a valley of a mountainous region. The mountains can shelter the valley from synoptic winds driven by large scale pressure gradients. This phenomenon enables the formation of local winds only driven by thermal effects. If synoptic winds are sufficiently weak, slope flows due to complex ground topography will influence the microclimate. This was mainly observed in the cities which are frequently subject to high pressure (Whiteman [1]).

Diurnal slope winds, driven by the differential heating of the Earth's surface, are generated by the horizontal temperature difference between air adjacent to a mountain slope and the ambient air at the same altitude over the neighbouring plane (or over the valley centre). The lack of thermal homogeneity is a consequence of the daily heating due to the solar radiation and to the nightly cooling related to the infrared radiation emitted by the ground. The slope flow is upslope (or anabatic) during the daytime and downslope (katabatic) during the nighttime. Anabatic winds break the environment stable stratification, while the nocturnal air sliding down origins a very stably stratified ambient at his bottom, the cold pool. Both anabatic and katabatic winds are typically in the range of 1-5 ms^{-1}, while their depth is in the interval 50-150 m for the anabatic winds and 10-40 m for the katabatic ones (Simpson [2]; Whiteman [1]). Both slope flows have a counter current compensating flow at higher height, which is directed in the opposite direction and has a lower velocity and a higher thickness. Those are difficult to observe with field measurements.

Starting from the theoretical study of Prandtl [3] and his analytical solution, numerous investigations have been proposed to analyze slope flows, using laboratory facilities (Hunt et al. [4], Fernando et al. [5]), field measures (Horst and Doran [6], Brehm and Freytag [7]), analytical models (Manins and Sawford [8], Horst and Doran [6]), numerical elaborations (Ye et al. [9], Tripoli and Cotton [10]). The urban heat

island was experimentally investigated by Lu et al. [11]. The interaction between the urban heat island and slope flows was studied via field measurements (Asaeda et al. [12]) and numerical investigations set-up with field measurements (Savijarvi and Liya [13]). Disadvantages of field studies are the high costs and the specific geometry in which measurements are performed. Results obtained by field studies are only applicable to the area where the measurement is performed, or to similar geometries. Numerical experiments are limited by computing capacity and are therefore not appropriate to investigate detailed phenomena. Analytical descriptions are only possible by applying restrictive assumptions. Laboratory-scale experiments could fill the gap among the limited computing capacity of numerical simulations, the lack of general applicability of field studies and the restrictive assumptions of analytical approaches. A major advantage of laboratory simulations is that the experimental parameters can be controlled separately. An important limitation of laboratory experiments appears to be the disability to match the aspect ratio of the UHI plume with the UHI plumes in field studies, owing to the reduced length scale of the experiment. Also because of the scale, individual buildings and street canyons cannot be resolved, and the characteristic Reynolds number of the simulated flow is several orders of magnitude smaller than that of the prototype. Thus, our model simulates only the large-scale circulation of the urban heat island within the boundary layer and ignores the detailed flow and heat-transfer phenomena within the canopy layer itself (Lu et al. [11]).

The purpose of this paper is to investigate specific aspects of slope flows and UHI-slope flow interaction via a laboratory apparatus reproducing the phenomenon in controlled temperature conditions. A simplified geometry for the slope with a plane tilted surface is assumed. Slope flows and UHI-slope flow interaction evolution will depend on ambient atmosphere thermal stratification gradient, heat flux along the slope and at the lower boundary, heat flux associated to the heat island. The combined use of thermocouples and flow visualization techniques provide the simultaneous measurement of temperature and velocity components. This then allows employing and cross-validating different methods to estimate the phenomenon evolution.

After the section devoted to the experimental setup description, results of the experiments are presented and compared to the theoretical models and state of the art. Finally, the concluding section draws the main outcomes of the experimental effort.

NOMENCLATURE

U	[-]	Averaged velocity
T	[K]	Temperature
z	[m]	Cartesian axis direction
g	[m/s^2]	Gravity constant
w_*	[m/s]	Convective velocity
w_D	[m/s]	Convective velocity for the UHI
D	[m]	Characteristic diameter of UHI
H_0	[W/m^2]	Surface heat flux
z_i	[m]	Inversion high
N	[s^{-1}]	Brunt-Vaisala frequency
h	[m]	Flow thickness
Ri_B	[-]	Bulk Richardson number
Fr	[-]	Froude number
$S_{1,2,3}$	[-]	Profile factor 1, 2, 3
c_p	[J/(kg*K)]	Specific heat capacity

Special characters

α	[rad]	Volumetric thermal expansion coefficient
β	[rad]	Slope angle
λ_U	[-]	Factor related to the depth of the surface layer
ρ_0	[kg/m^3]	Averaged fluid density
Δ	[m/s^2]]	Averaged buoyancy

Subscripts

a	Ambient
M	Mixed layer

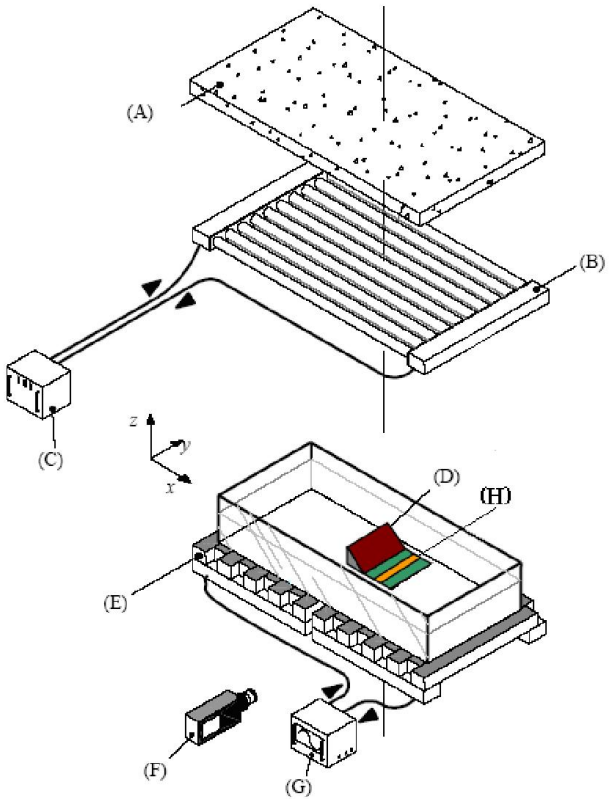

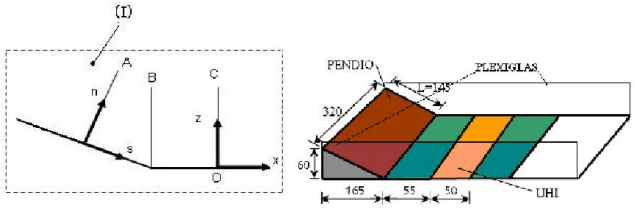

Figure 1 Experimental apparatus: A) polystyrene sheet, B) Free surface heat exchanger, C) Free surface thermostat, D) Valley model, E) Bottom surface heat exchanger, F) Camera, G) Bottom surface thermostat, H) rectangular- shaped electric heater , I) Reference systems and locations of temperature arrays velocity profiles (units are in mm)

EXPERIMENTAL SETUP

The experimental setup includes a tank of dimensions $1700 \times 600 \times 210$ mm³. A schematic of the flow field facility is shown in Figure 1 as well as the reference systems and locations of temperature measurement points and velocity profiles. In particular, profile A is in the middle of the slope, profile B at the slope bottom and profile C in the flat area 80 mm far from the slope bottom. To allow optical access, the lateral sides of the tank are made up of thick transparent glass. The temperature of the tank bottom and upper surfaces can be controlled by two heat exchangers allowing an approximately uniform thermal stratification of the needed intensity to be obtained in the water tank. A nearly linear vertical stratification profile, reached after about 16 hour, simulates a stably stratified environment in potential temperature. A polystyrene sheet is placed over the top of the tank to reduce heat losses.

A flat aluminium plate simulating the slope is mounted above the bottom surface. The plate inclination angle is $\beta = 20°$. Heating during the daytime and cooling during the nighttime experienced by the slope surface is simulated by means of a series of Peltier cells attached to the inclined plate. The surplus of surface heat flux between the city and its rural environment is simulated by means of a thin, rectangular- shaped electric heater built in a plastic tape of dimension 30×5 cm², connected to a suitable power supply. During the experiments aimed at investigating the anabatic currents, the test section bottom surface was heated to start and sustain convection.

Information about flow kinematics is achieved by using software packages based on Feature Tracking (Miozzi [14], Moroni and Cenedese [15]), a non-intrusive technique based on tracking of non-buoyant particles (pine pollen, ~80 μ m in diameter) recorded by high spatial (1728×2352 pixels) and temporal (up to 60 fps) resolution CMOS cameras. The measurement plane is illuminated by a high power linear light source. The instantaneous, two-dimensional velocity field is measured with a time resolution of 1/10 s. Temperatures are measured using 27 J-Type thermocouples mounted on three rakes placed at representative locations in the flow (Figure 1). The thermocouples are equally spaced every 2 mm in the vertical direction from 0 to 18 mm. A further array of 23 thermocouples, covering the entire water depth, is used for measuring the temperature distribution before the beginning of the experiment. The accuracy of the temperature data is 0.1 °C and the frequency of the data collection is 1 Hz. Disturbances on the velocity field produced by the racks of temperature sensors are minimized by positioning the racks in a plane parallel to the one illuminated by the light source, placed at a distance of nearly 50 mm.

Table 1 presents the values of characteristic quantities adjusted in the experiments.

Exp #	Experiment description	Gradient stratification (°C/cm)	Slope heat flux (kW/m²)	UHI heat flux (kW/m²)
1	Anabatic	1.0	1.0	-
2	Katabatic	1.0	1.0	-
3	Anabatic + UHI	1.0	1.0	0.6

Table 1 Experiment parameters. Time t=0 corresponds to beginning of image and temperature acquisition; for Exp # 1 and Exp # 2 heat is provided along the slope from t=20 s; for Exp # 3 the UHI heat flux begins at time t=2 s and heat is provided along the slope from t=120 s; in Exp # 1 and Exp # 3 the bottom is heated from t=2 s from the beginning of the experiments to start and sustain convection

RESULTS

Here we present velocity fields and vertical profiles for the three cases described in Table 1. For Exp #1 and Exp #2 the temperature profiles along the slope are compared. The velocity fields have been obtained by interpolating on a regular grid the velocity data output by Feature Tracking. The mesh size is 2.5 mm×2.5 mm superimposed to a region of dimensions 23×7 cm², resulting in 92×28 knots. These velocity data have been averaged over time intervals equal to or 2 seconds (20 frames) when the aim was to highlight turbulent structures or 20 seconds (200 frames) to visualise the average circulation. When the velocity field averaged over the smaller time intervals is analogous to the one averaged over the larger one, the former is presented. Velocity profiles have been computed by interpolating along a line sparse velocity data output by FT with a spatial resolution of 1 mm and

a time interval of 20 seconds. For profile location within the slope- valley system refer to Figure 1. The reference system axis s is positive oriented downslope.

Figure 2 describes the mean velocity fields relative to Exp #1 (anabatic case without heat island). The upslope flow is well visible in Figure 2b and 2c and less in Figure 2a which describes the phenomenon when the slope heating is just started and the incoming flow is very slow. The air motion is almost horizontal in the valley while it reaches the top of the slope through eddies structures which move upslope (Figure 2c). They form from the incoming of convective cells driven upslope by the pressure gradient along the slope (Princevac and Fernando [16]). This flow feature can be visualized only when the velocity fields are averaged over small time interval, 2 seconds in this case. The compensating flow slowly sliding upon the anabatic flow can be observed as well.

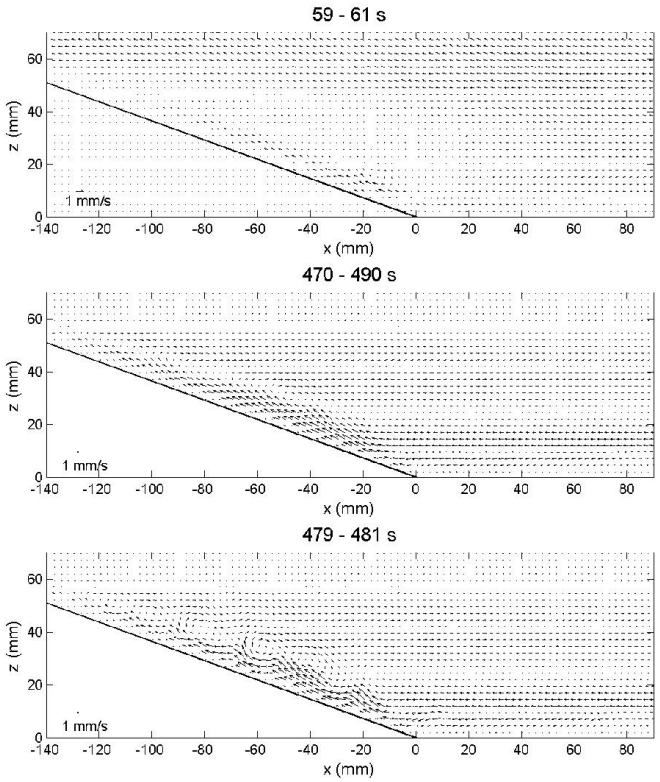

Figure 2 Mean velocity fields after (a) 60 s (average over 2 s); (b) 480 s (average over 20 s); (c) 480 s (average over 2 s) from the beginning of Exp #1

Figure 3 compares the velocity component along the slope (profile A) and the horizontal velocity (profiles B and C) for Exp #1. The steady state occurs about 120 s after the heating starts. After 120 s, velocity and flow thickness variations are small, presenting only oscillations. In the middle of the slope, the tangential velocity rapidly increases till 120 s and becomes roughly constant until 600 s. The maximum value is 1.6 mm/s while the maximum thickness is of about 10 mm. The same behaviour can be observed in the other two profiles where the maximum velocity value is smaller (1.2 mm/s at the slope base and 1.1 mm/s in the flat area downhill) and the current thickness is larger (between 26 and 22 mm at the beginning and at the end of the experiment for the slope base and between 26 and 19 mm in the flat area downhill) while it decreases reaching the end of the experiment. The anabatic current appears then thicker at the base of the slope than at the slope centre, and it is slightly thicker in the valley centre. Consistent is the counter current compensating flow of roughly 40 mm thickness and 0.60 mm/s maximum velocity value.

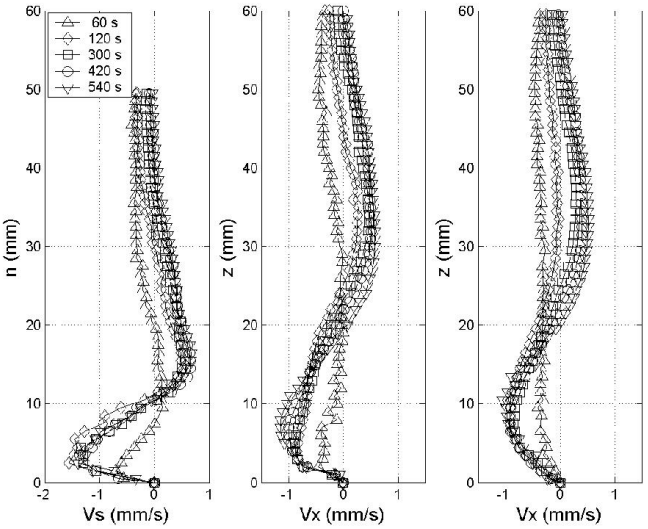

Figure 3 Velocity profiles A, B and C and 4 time intervals from the beginning of Exp #1.

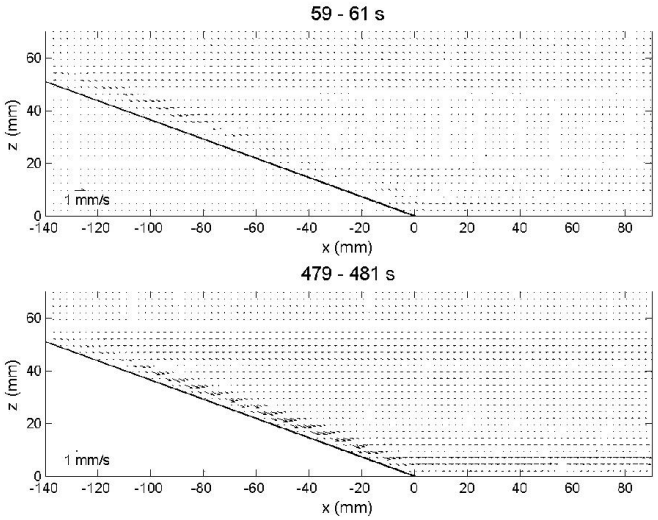

Figure 4 Mean velocity fields after (a) 60 s (average over 2 s); (b) 480 s (average over 2 s) from the beginning of Exp #2

Figure 4 describes the velocity fields for Experiment #2 (katabatic case without heat island). The time interval for data averaging does not influence the results. For this reason, velocity maps obtained averaging data over 2 second are presented. This implies the system was unable to capture the turbulent structures characterising the interface between the principal current and the compensating flow. The velocity field maps show a down- slope flow determining water cooling towards the bottom of the slope. Cold water flows in the same direction along the valley. Analogously to Exp. #1 the compensating flow can be observed but it is weaker and nearly horizontal.

Figure 5 compares the velocity component along the slope (profile A) and the horizontal velocity (profiles B and C) for Exp #2. The velocity increases with time, quickly for earlier times (from 60 s to 120 s from the beginning of the experiment) and more gradually in the remaining time lag. Then, in this case, the steady state is not reached. The maximum value of the velocity component along the slope on its centre (profile A) reaches 2 mm/s, resulting much greater than the horizontal component at the base of the slope (profile B; maximum velocity value equal to 0.8 mm/s) and at the flat area downhill (profile C; maximum velocity value equal to 0.9 mm/s). The flow thickness in the middle of the slope is substantially constant with time to a value of about 8 mm. The thickness variations are negligible even for the other two profile locations (the thickness in B is around 20 mm whereas it is about 15 mm in C), at the base of the slope is greater than that in the valley centre. The compensating flow is visible upon the katabatic wind, and it is characterized by lower velocity values (0.4 mm/s) and higher thickness than the down- slope flow.

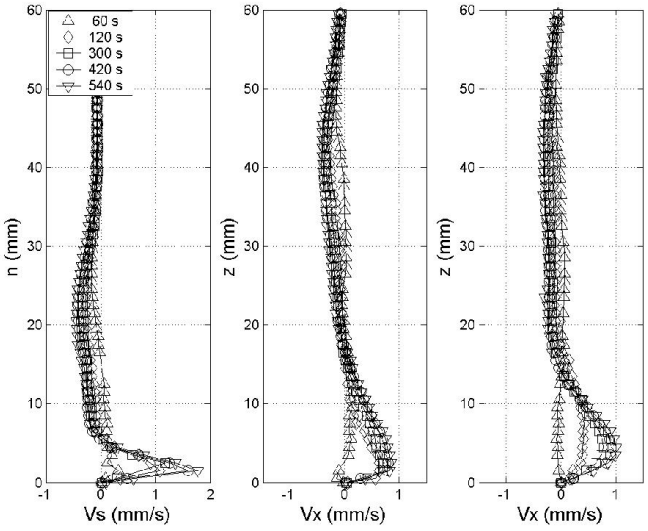

Figure 5 Velocity profiles A, B and C and 4 time intervals from the beginning of Exp #2

Figure 6 describes the velocity fields relative to Exp #3 (anabatic case with heat island). The initial 120 s are characterized by the urban heat island in a stratified environment only. The slope heating starts after 120 s from the beginning of the experiment. The urban heat island plume can be observed in Figure 6a, while in Figures 6b and 6c the upslope flow deforms the plume by bending. The plume is then displaced and destroyed. The heat surplus provided at the UHI location then contributes to the recirculation zone localised about 25 mm to the left of the central position of the resistance. The remaining flow is organized in eddies sliding along the slope, as in the anabatic case without urban heat island. The velocity component along the slope increases with time starting from 120 s to 240 s after the beginning of the experiment, i.e. 120 s after the heating starts. Also in this case the steady state is reached after about 120 s.

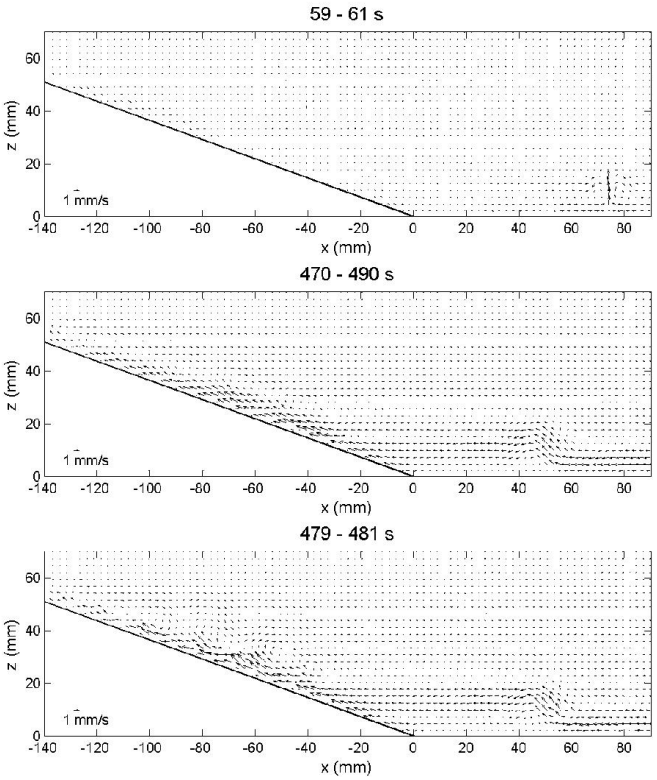

Figure 6 Mean velocity fields after (a) 60 s (average over 20 s), (b) 480 s (average over 20 s), (c) 480 s (average over 2 s) from the beginning of Exp #3

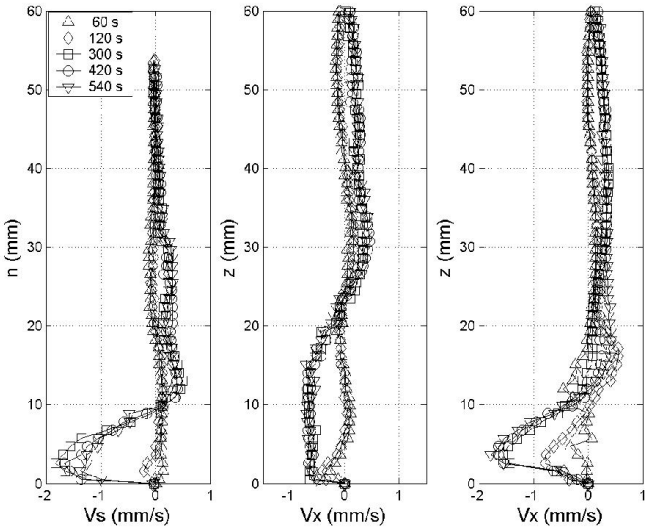

Figure 7 Velocity profiles A, B and C and 4 time intervals from the beginning of Exp #3

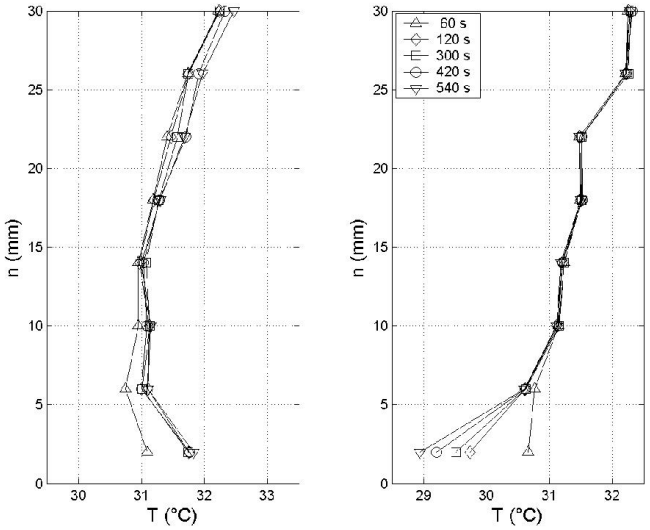

Figure 8 Temperature profiles A, B and C and 4 time intervals from the beginning of Exp #3

Figure 7 compares the velocity component along the slope (profile A) and the horizontal velocity components (profiles B and C) for Exp #3. Profile A shows the anabatic current starts after 120 s from the beginning of the experiment. Velocity quickly increases until 240 s and slows down until 480 s reaching 2 mm/s. The velocity distribution is similar to Exp #1, with larger velocity values. Profile B clearly shows the rapid increase of the horizontal velocity after the slope heating starts and the interaction with the urban heat island disturbing the horizontal flow directed from the flat area downhill to the slope. The profile, evidently different than Figure 3, then reflects the effects of turbulent mixing which tends to homogenize quantities in the vertical direction. After 240 s, the velocity profile presents an almost uniform value roughly equal to 0.7 mm/s, for a depth of 15 mm. Higher, velocity linearly decreases till - 0.5 mm/s. The velocity is null at distance larger than 20 mm from the lower boundary. Velocity increases quickly until 240 s and moderately until 480 s. The flow thickness doesn't change substantially in time both at the slope base and centre, but its value is much greater at the base, while its velocity is much lower. The effects of the anabatic wind on the urban heat island can be summarized as follows (profile C): the horizontal velocity component is almost null for the initial 60 s, then (until 180 s) the profile changes assuming the characteristic shape of the velocity distribution expected within a plume, close to its centre; after 180 s, when the anabatic current is well established, the velocity increases and the profile shape resembles the one reconstructed along the slope with a comparable maximum velocity value. The anabatic layer thickness is more than 10 mm. The return current is similar to the one reconstructed for Exp #1.

Figure 8 presents the temperature profile A for the anabatic and the katabatic current without urban heat island. In the anabatic case, the temperature increase manifests itself principally close to the slope surface and until about 15 mm far from the lower boundary. The maximum temperature variation is +1.6 °C. At larger heights, temperature profiles uniformly shift toward warmer temperatures (maximum temperature increase of 0.35 °C). For the katabatic case, the effects of the heat exchange between the bottom surface and the fluid are clear until about 8 mm. The temperature decrease (reaching the maximum value of 2 °C) is abrupt during the initial 120 s, whereas it becomes gradual till the end of the experiment.

COMPARISON WITH THEORETICAL MODELS AND STATE OF THE ART

Hunt et al. [4] derived a theoretical model valid for fully developed up- slope flows. The model assumes the boundary layer divided into three sub-layers, namely, a surface layer, a middle layer and an inversion layer. In each of these sub- layers the momentum and the heat equations written in terms of mean quantities are solved, matching the results at the boundary of each sub- layer to the next. Closures based on level- terrain turbulence parameterizations are used in the theoretical model. A mean upslope flow velocity of the form:

$$U_M = \lambda_U w_* \beta^{1/3} \qquad (0)$$

can be derived. Here λ_U is a factor related to the depth of the surface layer, $w_* = \left(\alpha g h H_0 / \rho_0 c_P\right)^{1/3}$ is the convective velocity, h is the convective layer depth, ρ_0 the average density of the fluid, c_P the heat capacity and H_0 the surface heat flux.

The comparison is allowed only for anabatic

currents. The experiments presented here (Figure 9) provide values of λ_u between 1 and 2, in good agreement with the other published in the literature.

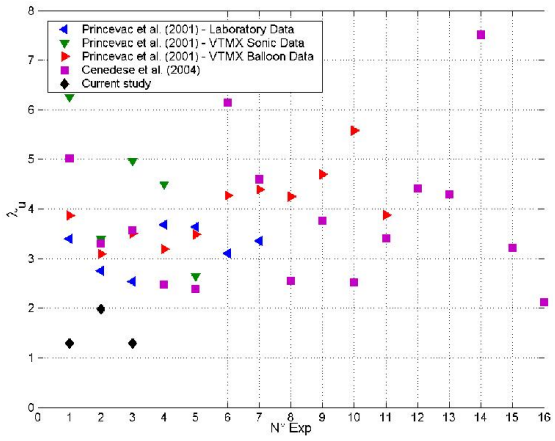

Figure 9 Comparison with Hunt et al. (2003) theoretical model.

Manins and Sawford [8] derived a model of katabatic winds based on the so-called "extended hydraulic approach", in which information on the flow structure along the direction normal to the slope is absorbed into three profile factors (S1, S2, S3) which are assumed known. S1, S2 and S3 take the value unity for well-mixed katabatic flow. Therefore, a layer with equivalent velocity, depth and buoyancy scales replaces the detailed structure of the flow. Compared with the Prandtl's theory, the analytic solution of the Authors [8] is valid also in non-stationary conditions and taken into account the entrainment of ambient fluid. The Bulk Richardson number (Ri_B) is employed for comparing data ($Ri_B = h \Delta \cos\beta / U^2$).

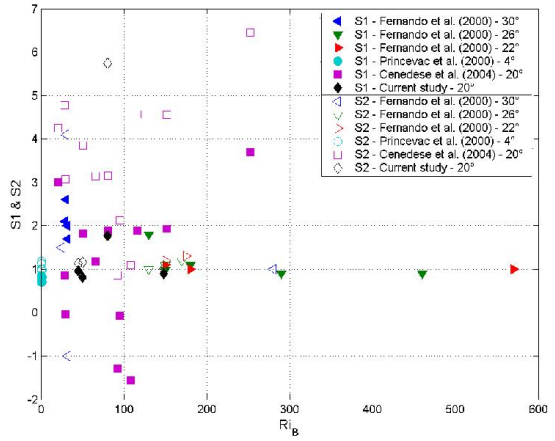

Figure 10 Comparison with Manins and Sawford (1979) theoretical model

S1 values, ranging between 0 and 4, spread out for small values of Ri_B, and are closer to 1 for large Ri_B. S2 values are more disperse for any value of Ri_B, ranging between 0 and 5. The present experimental effort provides S1 values slightly lower than 1, S2 values slightly larger than one to be compared to S1=0.5 and S2=0.9 provided by the Authors [8].

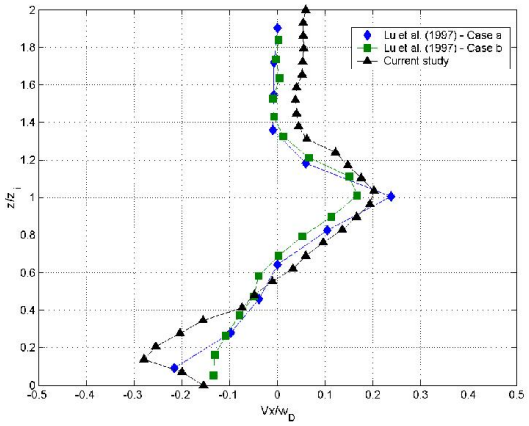

Figure 11 Non-dimensional horizontal velocity component profiles at location C.

The bulk convection model proposed by Lu et al. [11] is employed to make comparisons for the UHI circulation of Exp #3. The Authors [11] show that, in calm and stably stratified conditions, UHIs induced by circular shaped cities can be modeled by means of three parameters, namely, the surface heat flux, the city diameter D and the ambient thermal stratification dT_a/dz (T_a is the ambient temperature). They also showed that the Froude number $Fr = U_D/ND$ is the only non-dimensional parameter governing the UHIs dynamics when the flow is fully turbulent. Here, $U_D = \left(\alpha g D H_0/\rho_0 c_P\right)^{1/3}$ is the horizontal velocity scale, $W_D = U_D Fr$ is the vertical velocity scale and $N = \left(\alpha g dT_a/dz\right)^{1/2}$ is the Brunt-Vaisala buoyancy frequency. The Lu et al. [11] theory was developed for circularly shaped low-aspect-ratio UHIs ($z_i/D << 1$, where z_i is the mixing height) characterized by an axisymmetric flow field.

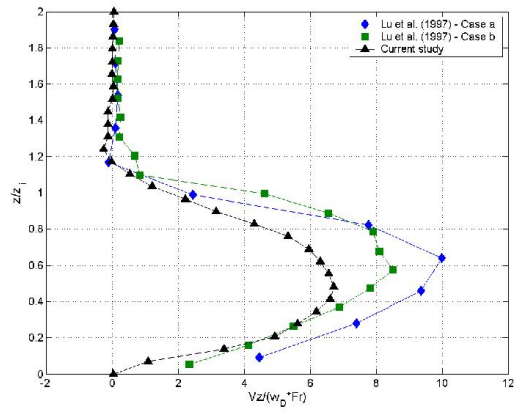

Figure 12 Non-dimensional vertical velocity component profiles at location C

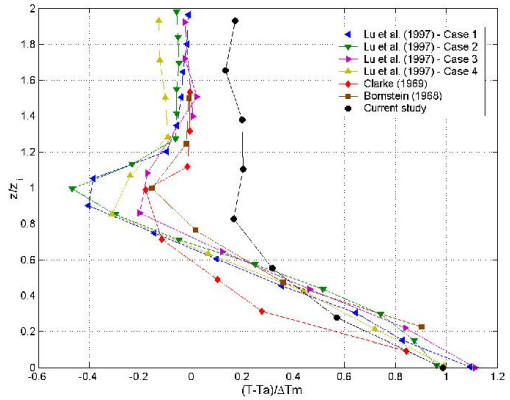

Figure 13 Non-dimensional mean temperature profiles at location C.

Here the horizontal and vertical velocity components profiles and temperature profiles are compared to corresponding profiles in [11]. The horizontal velocity components are close but close to the lower boundary and in the upper portion of the plume where the presence of the anabatic current at the beginning of its development produces velocity values different than zero. The temperature profile nicely collapses on the reference ones until roughly half the plume height. For larger heights, the temperature profile is close to zero.

CONCLUSIONS

In the case of anabatic winds, air goes up along the slope forming eddies structures that move upslope. In the case of katabatic winds, the flow thickness increases toward the slope base. The interaction of the anabatic flow with the urban heat island determines the deformation of the horizontal flow sliding along the valley to the slope; this diverges on top and assumes a quasi uniform vertical distribution of the horizontal velocity component, with a maximum velocity value very low, until the slope is reached. The upslope flow originates a horizontal motion in valley, that tilts the plume structure due to the urban heat island.

These effects are similar to those observed in the experimental investigation of the interaction between urban heat islands and sea breezes (Cenedese and Monti [17]).

REFERENCES

[1] Whiteman C.D., Mountain meteorology: fundamental and applications, *Oxford University Press,* 2000, 355 pp.

[2] Simpson J.E., Sea breeze and local winds, *Cambridge University Press,* 1994, 234 pp.

[3] Prandtl L., Essentials of fluid dynamics, *Hafner,* 1952, 422-425 pp.

[4] Hunt J.C.R., Fernando H.J.S., and Princevac M.., Unsteady thermally driven flows on gentle slopes, *Journal of Atmospheric Sciences,* Vol. 60, 2003, pp. 2169-2182.

[5] Fernando H.J.S., Princevac M., Hunt J.C.R., and Pardyjak E.R., Thermal circulation in complex terrain: a case of urban fluid mechanics, *Proceedings of the 5th International Symposium on Stratified Flows,* Vancouver, Canada, 10-13 July, 2000.

[6] Horst T.W., and Doran J.C., Nocturnal drainage flow on simple slopes, *Boundary-Layer Meteorology*, Vol.34, 1986, pp.263-286.

[7] Brehm M., and Freytag C., Erosion of the Night-Time Thermal Circulation in an Alpine Valley, *Archives for Meteorology, Geophysics, and Bioclimatology*, Ser. B, Vol. 31, 1982, pp. 331-352.

[8] Manins P.C., and Sawford B.L., A model of Katabatic winds, *Journal of Atmospheric Sciences*, Vol. 36, pp. 619-630, 1979.

[9] Ye Z.J., Segal M., and Pielke H.L., Effects of Atmospheric Thermal Stability and Slope Steepness on the Development of Daytime Thermally Induced Upslope Flow, *Journal of Atmospheric Sciences*, Vol. 44, n. 22, 1987, pp. 3341-3354.

[10] Tripoli G.J., and Cotton W.R., A numerical study of an observed orogenic mesoscale convective system. Part I: simulated genesis and comparison with observations, *Monthly Weather Review*, Vol. 117, 1989, pp. 273-304.

[11] Lu J., Arya S.P., Snyder W.H., and Lawson Jr. R.E., A Laboratory Study of the Urban Heat Island in a Calm and Stably Stratified Environment. Part I: Temperature Field - Part II: Velocity Field, *Journal of Applied Meteorology*, Vol. 36, 1997, pp. 1377-1401.

[12] Asaeda T., Fujino T., and Armfield S.W., Characteristics of Urban Heat Island in a City Located at the Bottom of Basin, *Proceedings of the 5th International Symposium on Stratified Flows,* Vancouver, Canada, 10-13 July, 2000.

[13] Savijarvi H., and Liya J., Local winds in a valley city, *Boundary-Layer Meteorology*, Vol. 100, 2001, pp. 301-319.

[14] Miozzi M., Particle tracking velocimetry using feature tracking and Delaunay tessellation, *Proceedings of the 12th International Symposium on Applications of Laser Techniques to Fluid Mechanics*, Lisbon, Portugal, 12-15 July, 2004.

[15] Moroni M., and Cenedese A., Comparison among feature tracking and more consolidated velocimetry image analysis techniques in a fully developed channel flow, *Measurement Science and Technology*, Vol. 16, 2005, pp. 2307-2322.

[16] Princevac M., and Fernando H.J.S., A criterion for the generation of turbulent anabatic flows, *Physics of Fluid,* Vol. 19, 2007, pp. 1-7 (105102).

[17] Cenedese A., and Monti P., Interaction between an Inland Urban Heat Island and a Sea-Breeze Flow: A Laboratory Study, *Journal of Applied Meteorology*, Vol. 42, 2003, pp. 1569-1583.